Reentrant Behavior in Binary Mixtures of (Octyloxy)cyanobiphenyl (8OCB) and the Shorter Chain Homologue (Heptyloxy)cyanobiphenyl (7OCB)

Mohamed B. Sied,[†] Josep Salud,[†] David O. López,*[,†] Hassan Allouchi,[‡] Sergio Díez,[§] and Josep Ll. Tamarit[†]

Laboratori de Caracterització de Materials (LCM), Departament de Física i Enginyeria Nuclear, ETSEIB Universitat Politècnica de Catalunya, Diagonal 647, 08028 Barcelona, Spain, Laboratoire de Chimie Physique, Faculté de Pharmacie, 31 avenue Monge, F-37200 Tours, France, and Departamento de Física Aplicada II, Facultad de Ciencias, Universidad del País Vasco, Apartado 644, E-48080 Bilbao, Spain

Received: July 18, 2002; In Final Form: November 4, 2002

The complete stable phase diagram of the two-component system (heptyloxy)cyanobiphenyl (7OCB) + (octyloxy)cyanobiphenyl (8OCB) was determined by means of modulated differential scanning calorimetry (MDSC), optical microscopy, and X-ray diffraction measurements. It was experimentally established that the 7OCB + 8OCB two-component system exhibits a monotropic reentrant nematic behavior. A complete quantitative thermodynamic analysis, through Oonk's equal *G* analysis, was performed, including the calculation of the monotropic reentrant behavior and a discussion of the stable melting phase diagram. Moreover, the specific-heat critical exponents (α), through second-order SmA to N transition, was obtained. If these α-values, together with those corresponding to other systems sharing cyanobiphenyl (*n*CB and *n*OCB) compounds, are plotted against the normalized nematic ranges, a common and uniform crossover trend is found. This behavior allows one to predict, in a simple way, the order of the SmA to N transition.

1. Introduction

Reentrant behavior in liquid crystals was first discovered nearly 30 years ago by Cladis.[1] On cooling of a sample from the isotropic phase (I), a nonstandard mesophase sequence—nematic (N), smectic A (SmA), and nematic again, named reentrant nematic RN—could be obtained, either by pressure in certain pure compounds[2,3] or by making appropriate mixtures of certain materials.[4−7] These liquid crystal materials display several common features: the constituent molecules have strongly polar end groups and a smectic layer spacing *d*, such that $l < d < 2l$ (where *l* denotes the length of the molecule). This kind of smectic is referred to a partial bilayer smectic, often denoted SmA_d.

The discovery of the reentrance phenomenon has resulted in extensive experimental and theoretical studies.[8,9] The first attempts to understand the reentrance were performed by Klug and Whalley[10] and independently by Clark,[11] who fitted the experimental results (temperature−pressure or temperature−composition) to either an ellipse or a parabola. Among the microscopic theories, maybe the most successful in reproducing the observed reentrant behavior was the *frustrated spin-gas model*.[12,13] A simple thermodynamic approach in reproducing and quantifying the reentrant nematic behavior in a two-component system was attained by Van Hecke[14,15] using Oonk's thermodynamic equal *G* analysis.[16]

From the thermodynamic point of view, reentrant nematic behavior seems to violate the often accepted, but never postulated, law that *less ordered phases should exist at higher temperatures than higher symmetry ones.* In fact, this phenomenon is not only limited to liquid crystals. Other examples of reentrance can be found in superconducting materials, vapor−liquid systems, ferroelectrics, etc.[9] In all these cases the return to a disordered state with decreasing temperature is caused by competing order parameters.

On the experimental side, several kinds of measurements such as specific heat,[5,7] X-ray diffraction,[4,17,18] optical,[4,5,19,20] birrefringence,[21] dielectric spectroscopy,[22] and high-resolution volumetric determinations[18,23] were performed on mixtures of some liquid crystals of the series of alkylcyanobiphenyls (*n*CB, where *n* denotes the number of carbons in the alkyl chain) and on (alkyloxy)cyanobiphenyls (*n*OCB, where *n* has the same meaning as the former) all of them known to exhibit SmA_d. In particular, the 6OCB + 8OCB mixtures have been broadly[4,5,17,18,21−23] studied, probably because it is one of the first two-component systems where reentrance was observed. One might expect that reentrance occurs for mixtures of compounds belonging to the same series or even to homologous series, chosen in such a way that a member without smectic phase is mixed with a member displaying SmA_d phase. Following this line of reasoning and if we focus on the *n*OCB series of compounds, the longest *n*OCB compound that does not display SmA_d is 7OCB, and so the 7OCB + 8OCB two-component system constitutes a likely candidate to display reentrant nematic. Similar arguments indicate that excellent candidates to display this phenomenon are, for instance, 6CB + 8CB or 7CB + 8CB. The latter was studied by Thoen et al.[24] nearly 20 years ago, and no sign of reentrance was reported.

In the work dealt with in this paper, we have carried out modulated differential scanning calorimetry (MDSC), optical, and X-ray diffraction measurements in order to completely characterize the 7OCB + 8OCB two-component system. The experimental results confirm the existence of a monotropic

* To whom correspondence should be addressed. E-mail: david.orencio.lopez@upc.es.
[†] Universitat Politècnica de Catalunya.
[‡] Faculté de Pharmacie.
[§] Universidad del País Vasco.

10.1021/jp021649o CCC: $25.00
Published on Web 07/04/2003

reentrant nematic phase. A complete thermodynamic analysis, particularly addressing the reentrant behavior, has been performed through the Oonk's equal *G* analysis. Likewise, and as a part of a work devoted to analyze the order of the SmA to N transition in the *n*CB and *n*OCB homologous series of compounds,[25,26] a high-resolution MDSC study has been also performed to obtain the specific heat data of some mixtures.

Kobayashi,[27] McMillan,[28] and de Gennes[29] explained, a long time ago, the order of the SmA−N transition. Assuming a coupling between nematic and smectic order parameters, they were capable to predict crossover behavior from the strict second-order 3D-*XY* transition, as well as the tricritical point (TCP) beyond which the first-order SmA to N transition occurs. In addition, McMillan, through the ratio T_{AN}/T_{NI}, also called McMillan's ratio (where T_{NI} is the nematic to isotropic transition temperature and T_{AN} is the smectic to nematic transition temperature), provided a simple quantitative criterion. The stronger the coupling occurs when McMillan's ratio is nearly 1. On the other hand, the 3D-*XY* model is only applicable when the nematic order is completely saturated. This takes place when the coupling is weak enough or, in terms of McMillan's ratio, when T_{AN}/T_{NI} is small enough. This value does not seem to be universal, being strongly material dependent (polar or nonpolar constituent molecules and mixtures between homologous, or not, series of compounds). Within this framework, is it possible to obtain a unique T_{AN}/T_{NI} value for an ensemble of like compounds, at which 3D-*XY* SmA to N transition is reached? And, if this is possible, is the same idea also applicable to the TCP? Going much farther away, is it also possible to find a common crossover behavior for an ensemble of like compounds? These are the basic questions that will be addressed within.

The paper is organized as follows. In section 2 we describe the experimental details. In section 3 a presentation of the information and results concerning the pure components 7OCB and 8OCB is made. In section 4, the experimental monotropic reentrant phase diagram is shown. In section 5, the thermodynamic analysis procedure and its results are presented. In section 6, the discussion is driven in two ways: first, a tentative stable melting phase diagram is proposed with the aid of the thermodynamic equal *G* analysis; second, the order of the SmA to N transition is discussed through the specific-heat critical exponent. Finally, in section 7, a summary of the main conclusions is made.

2. Experimental Section

2.1. Materials. The pure components 7OCB and 8OCB were synthesized and purified by Prof. Dabrowsky in the Institute of Chemistry, Military University of Technology, Warsaw, Poland. The purity was stated to be higher than 99.9%, and no further purification was made.

Liquid crystal binary mixtures of 7OCB + 8OCB were prepared at room temperature by weighing the pure components in selected proportions. To obtain homogeneous mixtures, samples were sealed in aluminum pans, heated to isotropic phase, and annealed for a period of several days.

2.2. Thermal Measurements. Thermal measurements were performed on a TA Instruments DSC 2920, equipped with modulated DSC (MDSC) and a refrigerating cooling accessory (200 K). The DSC cell was purged with a dry helium flow.

The MDSC technique enables one to perform measurements as in a conventional DSC calorimeter, as well as in modulated mode. In such a mode, the conventional temperature program (usually a linear-time temperature program) is superimposed with a periodic temperature change (usually sinusoidal) which constitutes the perturbation. The response is embodied in the heat flow rate that, by means of an appropriate mathematical procedure, can deconvolute the response to the perturbation (a dynamic component arising from the temperature modulation) from the response to the conventional linear-time temperature program (an underlying heat flow rate, which is approximately the conventional DSC heat flow). This technique provides the ability to measure, under suitable conditions (linear response and steady state), the specific heat directly in a single experiment and to measure it even at very slow underlying heating rates. Its design makes it also suitable for quantitative measurements of latent heats of first-order transitions, even if they are weak. In addition, by measurement of phase shift changes (like in the AC technique), MDSC provides an intrinsic method to determine the character of a phase transition.[26] This method proved to be useful in the past in AC calorimetry.[31−33] In fact, there exists a relationship between the AC-phase shift δ and the MDSC-phase shift ϕ, normally, $\delta = (\pi/2) - \phi$. More details on the MDSC technique can be found somewhere else.[26,34−36]

Two sorts of MDSC measurements were made. In one type, cooling was performed from the isotropic phase (or heating from SmA phase), with the scanning rate 1 K·min^{-1}, the modulated temperature amplitude ±0.5 K, and the modulation period 60 s. The second batch of measurements consisted in heating from the SmA phase at 0.01 K·min^{-1}, with a modulation temperature amplitude of ±0.035 K and a period of 25 s. In both cases, the chosen parameters enabled one to obtain a linear response and a steady state. The sample masses were selected to ensure a uniform thin layer within the aluminum pan. The specific heat calibration was performed using pure synthetic sapphire, although the absolute accuracy is usually not better than 5% or even worse.

To obtain the complete two-component system, standard DSC measurements were made on various selected mixtures and pure components. The scanning rates were 2 K·min^{-1}, and the sample masses were chosen between 5 and 10 mg.

2.3. Optical Measurements. The microscopy observations were made with an Olympus polarizing microscope equipped with a Linkam THMSG-600 hot stage and a Linkam TMS-94 temperature controller. The sample cell from Linkam, with a thickness of 5 μm, was filled by capillarity with the liquid crystal in its isotropic phase. This kind of cell enables one to obtain an almost perfect parallel alignment. The cooling and heating rates were 2 K·min^{-1}.

2.4. X-ray Powder Diffraction. X-ray powder diffraction data were collected using a horizontally mounted INEL cylindrical position-sensitive detector (CPS-120) equipped with a liquid-nitrogen OXFORD cryosystems 700 series Cryostream Cooler (80−400 K). The detector used in Debye−Sherrer geometry consisted of 4096 channels. The angular step was 0.029° (2θ). Monochromatic Co Kα_1 radiation was selected (λ = 1.7889 Å). The sample was introduced into a 0.5 mm diameter Lindemann glass capillary and was rotated around the θ axis during the experiment. External calibration using sodalite and silver behenate was performed to convert channels to 2θ degrees by means of cubic spline fittings, to correct the deviation from angular linearity in PSD. DIFRACTINEL software was used for the calibration and for the peak position determinations after pseudo-Voigt fittings of the standard measurements.

Data were collected at different temperatures during acquisition times of 60 min. The slew rate was 1 K·min^{-1}, with stabilization time of 10 min at each temperature before data acquisition.

TABLE 1: Thermal Properties of Pure 7OCB and 8OCB

	Cr → SmA (or N)		SmA → N		N → I		
compd	*T*, K	Δ*H*, kJ·mol^{-1}	*T*, K	Δ*H*, kJ·mol^{-1}	*T*, K	Δ*H*, kJ·mol^{-1}	refs
7OCB	326.65	28.88			348.15		39
	323.71	28.07			349.38	0.54	40[a]
	326.65				347.75	0.25	41
					346.65		42
					347.2		43
	327.15	29.00					44
	327.22	29.20			347.85	0.31	this work[b]
8OCB[c]	327.68[b]	26.65[b]	340.37[d]	<0.03	353.39[d]	0.63	25

[a] DSC measurements at 5 K·min^{-1} in ref 40. A literal transcription was made. [b] Measurements at 2 K·min^{-1}. [c] A brief summary of the available thermal information on 8OCB from different bibliographic sources was made in refs 25 and 26. We consigned our experimental results published in ref 25. [d] MDSC measurements at 0.01 K·min^{-1}.

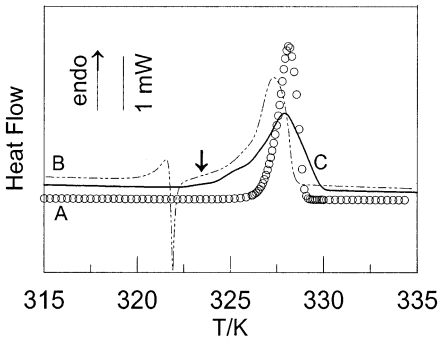

Figure 1. Melting DSC thermograms on heating for 7OCB. Curves A−C correspond to the melting of the most stable crystalline phase, metastable needle crystalline phase, and metastable collapsed crystalline phase, respectively.

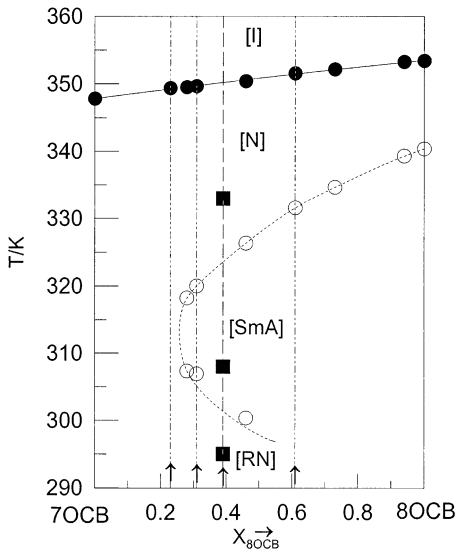

Figure 2. Partial phase diagram for 7OCB + 8OCB mixtures showing monotropic reentrant behavior. The dashed line and empty circles correspond to a second-order transition. Black circles and the continuous line correspond to a first-order transition. Black squares and vertical dot−dashed lines correspond to a set of microscopic measurements and three representative mixtures (for which specific heat data are reported), respectively.

3. Pure Components

Pure 8OCB exhibits, on heating from room temperature, the following phase sequence: Cr−SmA−N−I. Nevertheless, its solid-crystalline polymorphism is rather complicated, as has been recently pointed out by Hori and Wu.[37] There exist four different crystalline phases, denoted by Hori et al. as *square-plate*, *needle*, and *parallelepiped* (all three metastable) together with the stable crystalline phase (Cr_{8OCB}) found in commercial powder samples. Unfortunately, its crystalline structure is unknown, and not even its lattice parameters have been obtained yet. The Cr to SmA and the N to I phase transitions are known to be first order whereas the SmA to N phase transition has been stated to be, with no doubt, second order in nature.[25,26,38] Table 1 shows the thermal information on these stable phase transitions.

As for the shorter chain homologue 7OCB, it presents on heating from room temperature a slightly different phase sequence, in which the SmA mesophase does not exist: Cr−N−I. Like 8OCB, 7OCB exhibits a rather complicated solid-crystalline polymorphism, as also pointed out by Hori and co-workers 6 years ago.[44] There exist three metastable phases, denoted as square-plate, needle, and an intermediate solid state obtained from a collapsed square-plate crystal. Again, the structure or lattice symmetry of the most stable solid-crystalline phase (Cr_{7OCB}), present in the commercial sample is unknown. Figure 1 shows the DSC heat flow at 2 K·min^{-1}, corresponding to the melting of the most stable solid (Cr_{7OCB} to N) which is known to be first order (curve A). Curve B corresponds to the heating from room temperature of the same sample just after cooling from the isotropic phase. The profile of curve B matches the one reported by Hori and co-workers[44] for the melting of the *needle* metastable solid. Therefore, when the sample is cooled from the isotropic mesophase, the *needle* metastable solid is obtained, instead of the most stable Cr_{7OCB}. Once the *needle* solid is cooled from the arrow (just after the exothermic peak; see Figure 1) to 290 K and is subsequently heated to the melting, curve C is obtained. This profile can be identified with that obtained by Hori et al.[44] for the *collapsed* metastable solid. It is important to realize that if an annealing is made at the temperature marked by the arrow (≈322 K), for about 1 day or more, the *collapsed* metastable solid transforms to the most stable solid.

As for the N to I transition of 7OCB, and despite pretransitional specific-heat effects near the transition, it is considered to be first order in nature.[45] Our thermal results along with those already published by other researchers are gathered in Table 1.

4. Reentrant Nematic Phase Behavior

In Figure 2, the partial phase diagram of 7OCB + 8OCB, showing a monotropic reentrant nematic (RN) behavior, is depicted. This figure includes transition temperatures for the RN to SmA, SmA to N, and N to I phase transitions obtained from MDSC calorimetry working in modulated mode (specific-heat data) as well as in standard mode (heat flow data). The full circles represent the temperatures of the N to I first-order transition for pure components and their mixtures. Although a

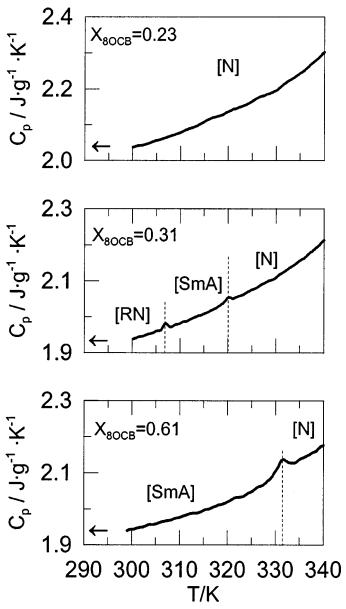

Figure 3. Specific heat data of three representative mixtures of the 7OCB + 8OCB two-component system. The data were obtained on cooling from the nematic mesophase.

two-phase equilibrium is experimentally found, it is very narrow (the MDSC technique allows one to observe a minimum coexistence region of 0.05 K wide) and, for simplicity, a single continuous line has been drawn. In contrast, when the transition is second order in nature, there is no phase coexistence region and only one line is required. This takes place at the SmA to N and also at the RN to SmA transitions, for which a dashed line has been plotted. Likewise, open circles have been used to represent second-order transitions.

The thermal measurements have been made on heating from room temperature and also on cooling from the isotropic phase. The RN phase has been detected for the first time on cooling, being a monotropic phase. In Figure 3, the trends in the specific-heat data for three representative mixtures are shown. As it can be observed for mixture $X_{8OCB} = 0.23$, no phase transitions have been detected from 340 to 300 K (the temperature about which the supercooled N mesophase crystallizes). A similar behavior was found for mixtures richer in 7OCB than $X_{8OCB} = 0.23$. On the other hand, for mixtures richer in 8OCB than the former, as for example $X_{8OCB} = 0.31$, two C_p peaks are observed on cooling: the higher in temperature corresponds to the N to SmA transition and the second, at lower temperature, corresponds to the SmA to nematic phase (denoted rentrant nematic RN), which was optically confirmed. Once the RN phase is formed on cooling, the reversible transition (RN to SmA) is observed on heating. Nevertheless, when the sample crystallizes, only the C_p peak corresponding to the SmA−N transition is detected on heating. The same monotropic behavior of the RN phase is observed for mixtures up to about equimolar composition. For mixtures with larger 8OCB content, like $X_{8OCB} = 0.61$ (see Figure 3) only one C_p peak is observed on cooling to 300 K, the temperature at which spontaneous crystallization of the supercooled SmA mesophase occurs.

The reentrant nematic was also evidenced optically, by means of a polarizing microscope. Figure 4 shows, as an example, the sequence on cooling from the nematic phase for the $X_{8OCB} = 0.39$ mixture in a parallel alignment. Figure 4A,C correspond to N and RN mesophases at 333 and 295 K, respectively. Figure 4B corresponds to the SmA mesophase at 308 K as can be

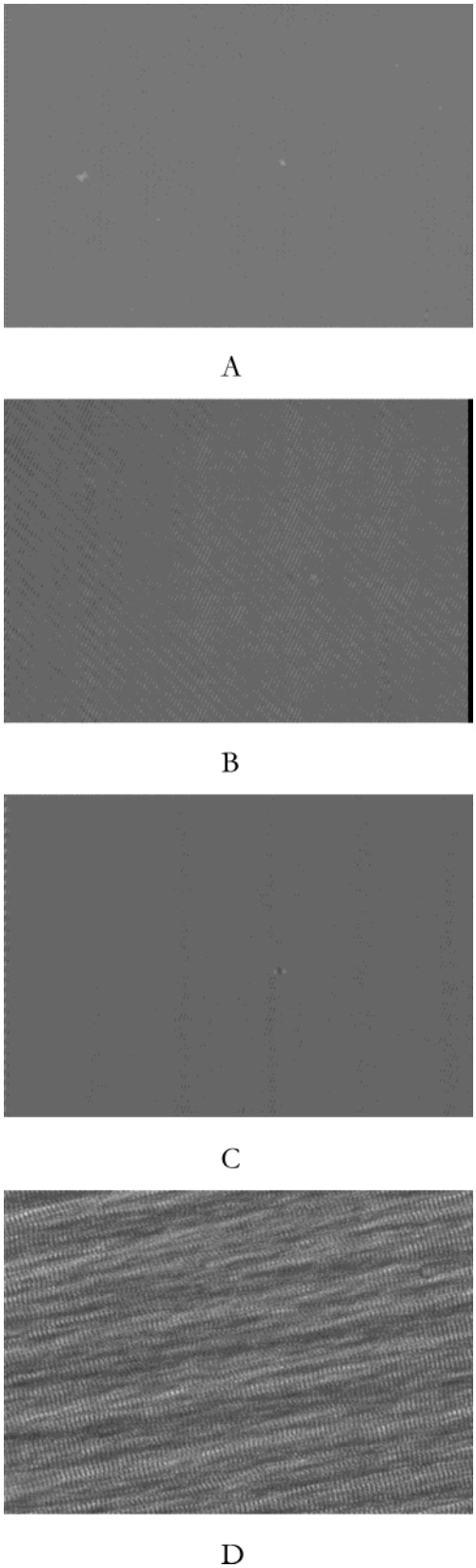

Figure 4. Evolution of mesophase structure for the mixture $X_{8OCB} = 0.39$ (parallel alignment) on cooling from isotropic phase: (A) nematic at 333 K; (B) smectic-A at 308 K; (C) reentrant nematic at 295 K; (D) crystal at 280 K. The (A)−(C) pictures correspond to the black squares in Figure 2.

inferred from the diagonal lines that correspond to the smectic planes. These temperatures were marked in Figure 2 by means

of black squares. Figure 4D shows the texture for the crystalline state obtained at about 280 K.

5. Thermodynamic Analysis

5.1. Thermodynamic Formulation and Methodology. Under isobaric conditions, the thermodynamic properties of a binary mixture of a two-component system A + B can be determined if, for each possible phase of this mixture, the molar Gibbs energy as a function of temperature andcomposition is known. The Gibbs energy function, in a phase α, is described by the following expression in terms of X moles of B and $1 - X$ moles of A (i.e. the mixture $A_{1-X}B_X$):

$$G^{\alpha}(X,T) = (1 - X)\mu_A^{*,\alpha}(T) + X\mu_B^{*,\alpha}(T) + RT[(1 - X)\ln(1 - X) + X \ln X] + G^{E,\alpha}(X,T) \quad (1)$$

Here $G^{E,\alpha}(X,T)$ is the excess Gibbs energy, $\mu_A^{*,\alpha}$ and $\mu_B^{*,\alpha}$ are the molar Gibbs energies of the pure components, R is the gas constant, and T is the thermodynamic temperature.

To determine an arbitrary two-phase equilibrium region, between two phases α and β, at each temperature in a two-component phase diagram, the traditional criterion of equilibrium is satisfied by the double tangent line to the minimum Gibbs energy functions giving rise to the equilibrium compositions (X_α and X_β). Sometimes, both compositions are very close and it results in a very narrow two-phase region. In addition, these compositions are very close to the intersection of both Gibbs energy functions, named equal Gibbs composition (EGC). This EGC changes with temperature, so giving rise to the equal Gibbs composition curve (EGCC or simply EGC curve),[16] which in a practical sense provides the representative line of the very narrow two-phase equilibrium in a $T-X$ plot. This situation takes place when the transition entropies of the pure compounds are very small, this being usual for many liquid crystal mesophase transitions. In the limit, in which the phase transition is purely second order in nature, the transition entropies of the pure compounds are considered to be zero, both equilibrium compositions and the EGC are equal, and no coexistence region exists.

Setting eq 1 for α-phase equal to its parallel for β-phase will give the EGC curve equation

$$G^{\alpha}(X,T) - G^{\beta}(X,T) = (1 - X)\Delta\mu_A^*(T) + X\Delta\mu_B^*(T) + \Delta G^E(X, T) = 0 \quad (2)$$

where $\Delta\mu_i^*(T) = \mu_i^{*,\alpha} - \mu_i^{*,\beta}$ (i = A, B). To proceed further, expressions are required for $\Delta\mu_i^*(T)$ and $\Delta G^E(X,T)$. For $\Delta\mu_i^*(T)$, using the transition temperature as a reference point, we have

$$\Delta\mu_i^* = -\Delta S_i^*(T - T_i) + \Delta C_{pi}^*(T - T_i - T\ln(T/T_i)) \quad (3)$$

where ΔS_i^* is the transition molar entropy change and ΔC_{pi}^* is the one in specific heat, both at the transition temperature T_i. It should be noted that ΔC_{pi}^* is taken to be the first-order difference in the specific heats between α and β phases. It should also be noticed that if the transition α to β were purely second order, ΔS_i^* would equal zero and $\Delta\mu_i^*$ is entirely determined by the change in specific heat.

For $\Delta G^E(X,T)$ a two-parameter form of the Redlich−Kister expansion is commonly used:

$$\Delta G^E(X,T) = X(1 - X)[\Delta A_1(T) + \Delta A_2(T)(1 - 2X)] \quad (4)$$

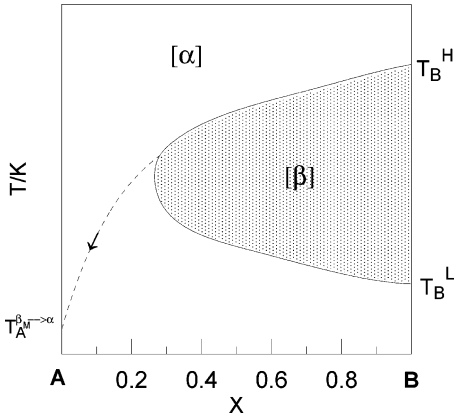

Figure 5. Qualitative two-component system exhibiting reentrant behavior. The possibility of a phase transition at a temperature lower than T_B^L is suggested by the dashed line.

Here $\Delta A_i(T)$ are usually taken to be constant or a function of temperature in the form $\Delta H_i^E - T\Delta S_i^E$.

The EGC method requires some experimental data related to the phase transition of the mixtures, to perform an iterative procedure in which one obtains a reasonable EGC curve as well as the $\Delta G^E(X,T)$ along this curve. This procedure can be automatically executed by means of the WINIFIT 2.0 software[46] (based upon MS-DOS LIQFIT and PROPHASE programs[47,48]), which also allows the calculation of the different compositions for each temperature at which transitions take place, that is to say, the complete phase diagram. The program was successfully tested in other two-component systems displaying first-[49−51] or second-order[25] phase transitions.

Reentrant phase behavior in an arbitrary two-component system A + B, as illustrated in Figure 5, can be also treated by means of the EGC method, as it was proposed by Van Hecke almost 20 years ago.[14] If compound B exhibits reentrant behavior for the phase α, temperatures T_B^H and T_B^L show successively (on cooling) the transitions α to β and β to α. On the other hand, for the compound A, which does not exhibit reentrant behavior, the possibility of a phase transition between α and β phases at a temperature lower than T_B^L is suggested by the dashed line in Figure 5. This phase transition can be also theorized as metastable, and WINIFIT software requires this input to perform the calculations.

A thermodynamic G analysis of the monotropic reentrant phase diagram depicted in Figure 2 must be performed by analyzing as a first step the [N + I] two-phase equilibrium, followed by the second-order SmA to N transition that exhibits a monotropic reentrant nematic behavior.

5.2. [N + I] Two-Phase Equilibrium. According to eq 1, one Gibbs energy function is needed for the I phase and another for the N phase. The required input for the theoretical analysis includes the experimental data points read from Figure 2, together with the experimental thermal properties of the pure components corresponding to the first-order N to I transition read from Table 1. The EGC method, via WINIFIT, provides the excess Gibbs energy difference between N and I phases along the EGC curve (given by an expression similar to eq 4) with the coefficients taken as temperature-independent:

$$\Delta G^E(X) = G^{E,I} - G^{E,N} = X(1 - X)[-3.68 - 1.16(1 - 2X)]\ \text{J·mol}^{-1} \quad (5)$$

This approach evidences that both N and I phases show almost the same deviation with regard to the ideal mixing behavior. Nevertheless, because of the small transition entropies of the

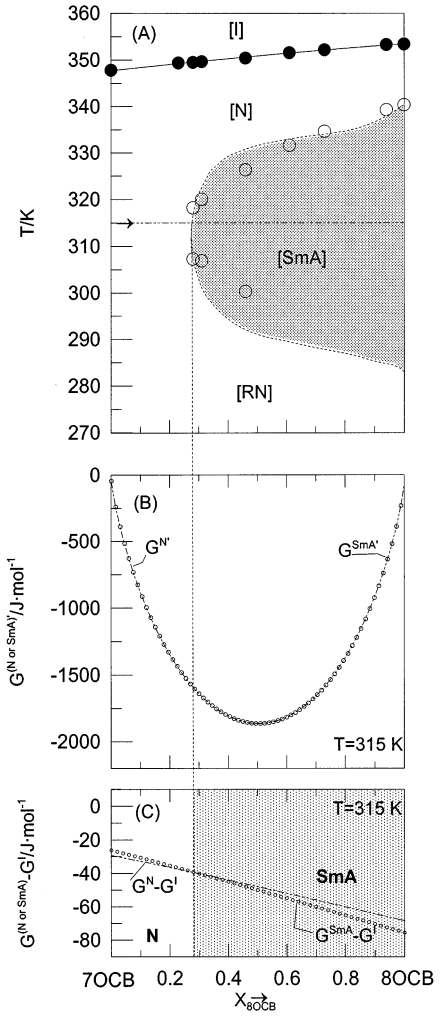

Figure 6. Calculated partial phase diagram for 7OCB + 8OCB mixtures showing monotropic reentrant behavior (symbols represent experimental information): (A) Gibbs energies of the mesophases (N and SmA) plus the linear contribution (see text); (B) Gibbs energy difference between the mesophase (N and SmA) and I; (C) both at 315 K.

pure compounds, the nonzero coefficients of eq 5 are seen to be necessary to accurately calculate the experimental two-phase equilibrium, as shown in Figure 6A. Nevertheless, phase I will be assumed to be strictly ideal in further calculations, and absolute values of the coefficients in eq 5 will be considered for the N phase. Finally, as this equilibrium is very narrow, only the EGC curve has been drawn for simplicity.

5.3. RN to SmA and SmA to N Transitions. The second-order SmA to N transition can also be calculated using WINIFIT by comparing the Gibbs energy curves of the N and SmA phases. To do so, a virtual SmA to N phase transition for 7OCB has to be considered for eq 2 to be applied. From the experimental data points of the mixtures for the SmA to N phase transition, WINIFIT software performs an estimation of the virtual or metastable transition temperature. The best value is calculated to be 280 K, a value that satisfies the condition that no transitions from SmA to N phase are allowed for 7OCB in the temperature range between T_B^H and T_B^L. Likewise, as this transition is considered to be second order, the entropy changes for both 7OCB and 8OCB compounds have to be set equal to zero or almost zero (experimental values are about 0.001 J·K·mol^{-1}). Thus, $\Delta\mu_i^*(T)$, given by eq 3, contains only the specific heat term (0.01 J·mol^{-1} K^{-1}) that was experimentally estimated for 8OCB from highly accurate specific-heat data.[25,26] The specific-heat change attributed to the virtual SmA to N transition for pure 7OCB was used as a parameter to be obtained from the present analysis. The value that provides the best adjustment is 0.002 J·mol^{-1} K^{-1}. Finally, the excess Gibbs energy obtained for the SmA phase is

$$G^{E,SmA}(X) = X(1-X)[3.67 + 1.15(1-2X)]\ \text{J·mol}^{-1} \quad (6)$$

In fact, the excess Gibbs energy difference between N and SmA phases is practically zero (about 0.0025 J·mol^{-1} at the equimolar composition), a result which had already been obtained for the two-component system 8CB + 8OCB.[25] The calculated EGC curve, drawn in Figure 6A, represents a strictly second-order transition line since no phase coexistence region exists. As can be observed, this calculated line reproduces the experimental reentrant nematic behavior. The T_B^L temperature, not experimentally accessible because of its supercooled metastable character, could be estimated to be 283 K.

The Gibbs energies G^N and G^{SmA}, built up by means of WINIFIT, scaled with respect to that of the G^I phase, that is to say, plus the linear contribution $-[(1-X)\mu_A^{*,I} + X\mu_B^{*,I}]$ (which just shifts both Gibbs energy values identically, while phase stability remains unchanged[16]). An example, at 315 K, is depicted in Figure 6B. As we can see, both *G*-curves appear to be identical. In Figure 6C, the same *G*-curves for which the term $RT[(1-X)\ln(1-X) + X\ln X]$ has been subtracted are shown. This picture enables us to better distinguish the small differences between both *G*-curves. In addition, the stability of the N phase with respect to the SmA phase is clearly observed for compositions lower than $X_{8OCB} \approx 0.3$ whereas, for compositions higher than that, the SmA is the most stable phase.

6. Discussion

6.1. Stable Melting Phase Diagram. The melting of both pure components, as has already been outlined in section 3, is rather complicated. In fact, the existence of several metastable solid-crystalline phases is the main problem when one tries to obtain the stable melting binary phase diagram.

The stable crystalline phases Cr_{7OCB} and Cr_{8OCB} are probably nonisostructural forms. If one keeps this fact in mind, the thermodynamic analysis of the melting phase diagram can be performed using the concept of crossed isodimorphism.[25,50,51] This assumes the existence of two-single loops [Cr_{7OCB} + N] and [Cr_{8OCB} + SmA] together with the second-order transition line, SmA to N, that has been calculated in section 5, crossing every other. An important part of the analysis consists of finding the metastable ends of these loops: the metastable transition point $Cr_{7OCB} \rightarrow$ N in pure 8OCB; $Cr_{8OCB} \rightarrow$ SmA in pure 7OCB. This information, experimentally unknown, usually can be extracted by extrapolating the known stable parts of related loops. Unfortunately, in the present case no reliable information on the stable parts seems to be available. For this reason, to obtain a solid−solid inmiscibility region between both Cr_{7OCB} and Cr_{8OCB}, in a first step the metastable transition points have been established. The calculated melting phase diagram is depicted in Figure 7. The full symbols denote DSC-experimental data. Previously, these data constituted unreliable information as no thermal signals characteristic of a eutectic three-phase equilibrium [Cr_{7OCB} + SmA + Cr_{8OCB}] had been found. Nevertheless, as we can observe from Figure 7, they actually correspond to the *liquidus* (the upper equilibrium line) of the [Cr_{7OCB} + N] and [SmA + Cr_{8OCB}] loops. This situation had already been found in the past for other disordered com-

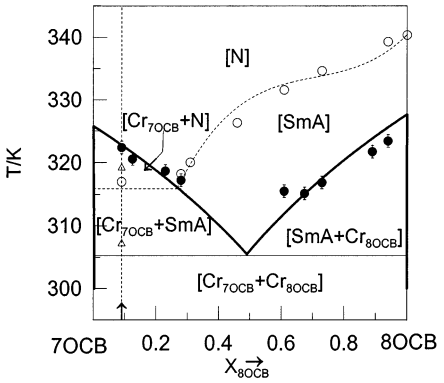

Figure 7. Tentative stable melting phase diagram for the 7OCB + 8OCB mixtures. The lines correspond to the thermodynamically calculated melting phase diagram. Black circles are DSC measurements, and triangle symbols correspond to X-ray diffraction measurements for the representative mixture ($X_{8OCB} = 0.09$ represented by the vertical dashed line). Empty circles and dashed lines correspond to a second-order transition.

pounds.[52−54] If this interpretation is correct, the analysis can be started again, but presently, by extrapolating the partially known stable parts of these loops. The chosen values for the metastable temperatures have been 200 and 265 K, for pure 7OCB (Cr → SmA) and 8OCB (Cr → N), respectively. Due to the lack of information, the melting entropy of each metastable crystalline phase was taken to be the same as that of the corresponding stable crystalline phase. It should be noted that the results of the analysis remain largely unchanged by modifications of the above metastable parameters, if no miscibility exists in the solid-crystalline state. The results, expressed as Redlich−Kister polynomials, are

$$G^{E,Cr7_{OCB}}(X) = X(1-X)[10000 + 100(1-2X)]\ \mathrm{J{\cdot}mol^{-1}} \quad (7a)$$

$$G^{E,Cr_{8OCB}}(X) = X(1-X)[10000 - 100(1-2X)]\ \mathrm{J{\cdot}mol^{-1}} \quad (7b)$$

The calculated melting phase diagram, depicted in Figure 7, represents the possible attainable phase equilibrium. However, we are not really certain whether this constitutes the stable melting phase diagram. Nevertheless in the following paragraphs we give additional arguments that would reinforce our *theory* of this possible attainable phase equilibrium.

From a theoretical point of view, the crossing between the [Cr_{7OCB} + N] liquidus line and the second-order transition line SmA−N leads to a *pseudoinvariant* line at 315.7 K ($0 \le X_{8OCB} \le 0.28$), where the [Cr_{7OCB} + SmA] coexistence domain would change to the [Cr_{7OCB} + N] one. This invariant temperature line does not represent one invariant in the strict sense because no coexistence of phases exists. In fact, pseudoinvariants like these are often unmarked on the reported phase diagrams. In Figure 8, the theoretical evidence for the existence of the pseudoinvariant is shown by means of the Gibbs energy curves built up using WINIFIT. Figure 8A,C shows the Gibbs energy curves G^{Cr7OCB}, G^{N}, and G^{SmA} (scaled with respect to that of the isotropic phase) at two temperatures, one below and one above the pseudoinvariant temperature. Again, no differences between G^{N} and G^{SmA} can be observed. As usual, the double tangent line provides the equilibrium compositions. The left X mol composition corresponds to $X_{8OCB} \approx 0$ for both temperatures (Figure 8A,C), whereas for the right X mol composition (for which, from Figure 8A,C, seems impossible to know the equilibrium phase) it corresponds either to the SmA or N mesophase. Again, to better discern the very small differences between the Gibbs energy functions of the SmA and N mesophases (Figure 8B,D) only the Gibbs energy functions of these mentioned phases (from which the term $RT\{(1-X)\ln(1-X) + X\ln X\}$ was subtracted) are shown. The stability domain of the SmA mesophase is shaded in Figure 8B,D, to make it stand out. The right equilibrium X mol compositions are thus clearly observed as SmA at 310 K and N at 318 K. Between 310 and 318 K, the pseudoinvariant is located as a second-order invariant line at which the SmA mesophase changes to the N mesophase, in the two-phase equilibrium region.

To determine this pseudoinvariant experimentally, an MDSC experiment was performed to obtain C_p data at 0.01 K·min^{-1} ($\Delta T = \pm 0.035$ K, $\tau = 25$ s, being the proposed conditions in section 2) on the mixture $X_{8OCB} = 0.09$. The binary mixture was stabilized at 306 K in the [Cr_{7OCB} + SmA] domain for a period of about 1 day. The C_p data are depicted in Figure 9. As it can be observed, a very small C_p peak is found in the vicinity of 317 K that is interpreted as the [Cr_{7OCB} + SmA] to [Cr_{7OCB} + N] second-order transition. A second C_p peak, in the vicinity of 320 K and larger than the first one, is interpreted as the [Cr_{7OCB} + N] to N transition. Moreover, an X-ray diffraction experiment on the same mixture, stabilized at 307.15 K for a period of about 1 day, was also performed to confirm the observed thermal behavior. Figure 10 shows the X-ray diffraction profiles in d spacing for the pure 7OCB at 307.15 K, together with those corresponding to the mixture $X_{8OCB} = 0.09$ at 307.15 and 319.15 K (below and above of the pseudoinvariant temperature, respectively). As it can be observed, the X-ray profile for the mixture at 307.15 K exhibits (at about 29 Å and overlapped with a peak corresponding to the Cr of 7OCB) the characteristic peak of the SmA mesophase, proving the coexistence of both the crystal and the SmA [Cr_{7OCB} + SmA] phases, at this temperature. On the contrary, at 319.15 K, only an enlarged peak is observed at about 28 Å, characteristic of the [Cr_{7OCB} + N] domain.

As for the eutectic three-phase equilibrium [Cr_{7OCB} + SmA + Cr_{8OCB}], the thermodynamic calculation leads to a temperature of 305.3 K; see Figure 7. No experimental evidence of such an invariant have been obtained because it is very difficult to obtain the demixing between both solid-crystalline stable phases, Cr_{7OCB} and Cr_{8OCB}, in a reasonable time span.

6.2. SmA to N Transition. The study of the second-order SmA to N transition was performed by measuring the specific-heat data of some binary mixtures at 0.01 K·min^{-1} ($\Delta T = \pm 0.035$, $T = 25$ s, the proposed conditions described in section 2). These C_p data were analyzed through the renormalization-group expression[45,55,56]

$$C_p^{\pm} = B + E\epsilon + A^{\pm}|\epsilon|^{-\alpha}[1 + D^{\pm}|\epsilon|^{0.5}] \quad (8)$$

where ± indicates above and below the transition. The temperature at which the smectic and nematic behaviors diverge is the critical temperature T_c. The reduced temperature is ϵ ($=(T - T_c)/T_c$). The corresponding amplitudes above and below are $A^{\pm}$, whereas the constants B and E account for the specific heat background, both being above and below the transition. The specific heat-critical exponent is α, also the same above and below the transition. The first-order correction to the scaling term is $D^{\pm}|\epsilon|^{0.5}$, which was added to the simple power law expression to guarantee the smooth variation of the background at T_c. We fixed the exponent of this term at the value 0.5 (essentially the 3D-XY value of 0.524 predicted for the model), and no additional fit was tried. The theory for the 3D-XY universality class predicts an amplitude ratio of $(A^-/A^+) = 0.971$,

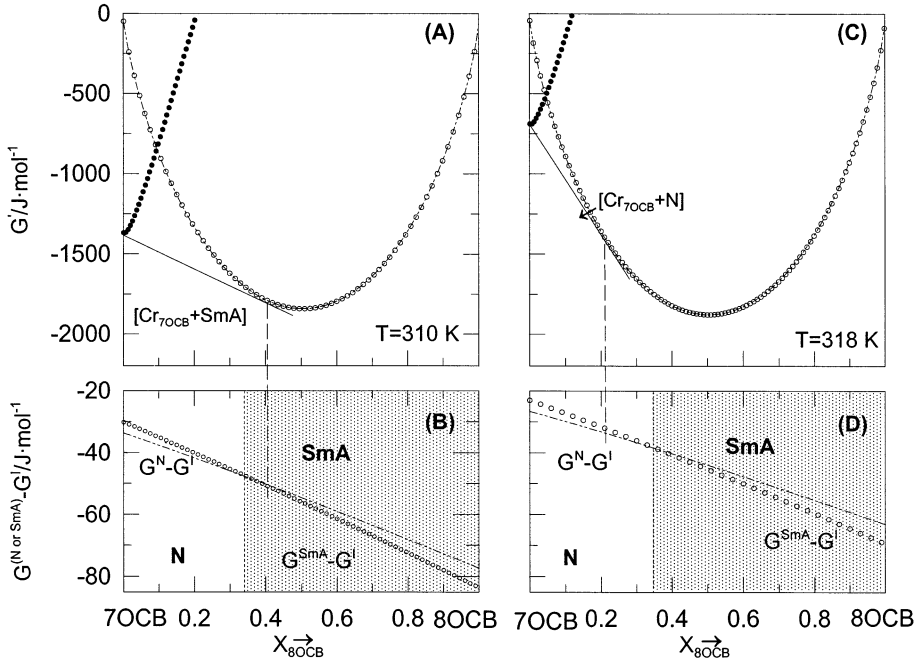

Figure 8. Gibbs energies of the mesophases (dot−dashed line, N; ○○○ line, SmA) and Cr_{7OCB} plus the linear contribution (●●● line) (see text) at (A) 310 K and (C) 318 K and Gibbs energy difference between the mesophase (dot−dashed line, N; ○○○ line, SmA) and isotropic phase I at (B) 310 K and (D) 318 K (D). In both (A) and (C), the double tangent lines to the Gibbs energy functions are pointed out. The (B) and (D) schemes represent the mesophase stability, SmA (shaded area) and N, respectively.

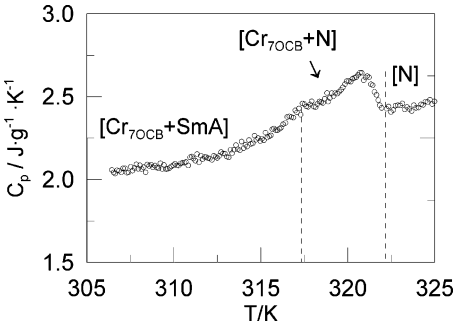

Figure 9. Specific heat C_p as a function of temperature for the mixture $X_{8OCB} = 0.09$ stabilized at 306 K for a period of about 1 day. The data have been obtained on heating.

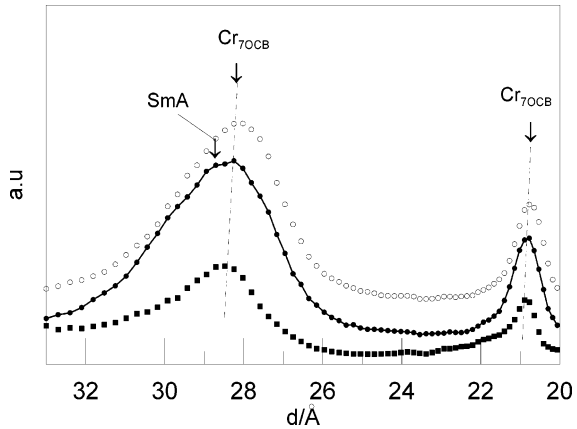

Figure 10. X-ray diffraction profiles for pure 7OCB at 307.15 K (■) and for the mixture of $X_{8OCB} = 0.09$ at 307.15 K (−●−) and at 319.15 K (○), respectively.

a critical exponent $\alpha = -0.007$, and $D^-/D^+ \approx 1$. These predictions are different around the TCP, where we have the theoretical amplitude ratio of (A^-/A^+) is about 1.6, the critical exponent $\alpha = 0.5$, and D^-/D is close to 1. Equation 8 is often used for pure liquid crystal compounds, although it can also be used for mixtures of homologous compounds.[26] Given that, for the mixtures dealt with in this work, the measurements are performed at constant mole fraction and no indications of Fisher renormalization are observed,[26,57] it seems physically reasonable that no significant distinction exists with regards to the measurements performed at constant chemical potential difference.

The results of fits using eq 8 (α, A^-/A^*, D^-/D^+, T_c), over the range $|\epsilon| \leq 5 \times 10^{-3}$, are presented in Table 2 for pure 8OCB and for the analyzed mixtures of the two-component system 7OCB + 8OCB. All the parameter sets represent well enough the measured specific heat data, as indicated by χ^2 values. For the mixture $X_{8OCB} = 0.61$, it was impossible to fit the α-critical exponent with the constraint $\alpha^+ = \alpha^-$. In fact, the greater the content in 7OCB, the smaller the C_p peak is, making it more difficult to perform the fit. As an example of the goodness of the fits, the result for the mixture $X_{8OCB} = 0.73$ is shown in Figure 11. It is interesting to note that this mixture is nearly 3D-*XY* since both the critical exponent α and the amplitude ratio (A^-/A^+) are close to the expected 3D-*XY* values (taking into account the quoted errors). In fact, the effective α values for the mixtures exhibit a common trend with varying composition, as we can see in Figure 12A. In addition, it seems to be that the 3D-*XY* model is reached for mixtures with 8OCB content slightly lower than 0.7 ($X_{8OCB} < 0.7$). As a consequence, for the fit corresponding to the mixture $X_{8OCB} = 0.61$ the critical exponent was fixed at a value of −0.007 (the theoretical 3D-*XY* value), while the other parameters were fitted according to eq 8. In Figure 12B, the nematic range NR ($=T_{NI} - T_{AN}$) normalized by T_{NI} (NR/T_{NI}) is also plotted against composition. As we showed not long ago in preceding papers[25,26] (for mixtures of the two-component systems 8OCB + 9OCB, 8CB + 9OCB, and 8CB + 8OCB), there exists a correlation between the effective α-values and NR/T_{NI} for the *n*CB and *n*OCB liquid crystals.

In Figure 13, the α-values of Figure 12 are plotted against their normalized nematic ranges. In addition, previously pub-

TABLE 2: Results of Fits to Eq 8 for Pure 8OCB and for Mixtures of the 7OCB + 8OCB Two-Component System[a]

X_{8OCB}	N	a	A^-/A^+	D^-/D^+	T_c, K	$10^3\chi^2$
0.61	182	−0.007[b]	0.7 ± 0.3	1.8 ± 1.1	331.59 ± 0.01	1
0.73	192	−0.001 ± 0.040	0.7 ± 0.5	0.7 ± 1.9	334.63 ± 0.01	2
0.94	269	0.043 ± 0.020	1.4 ± 0.5	0.7 ± 1.5	339.30 ± 0.02	5
1 (8OCB)[c]	286	0.044 ± 0.002	1.01 ± 0.01	0.6 ± 0.2	340.37 ± 0.01	1

[a] *N* is the number of data points included in these fits. The errors quoted are the statistical uncertainties. [b] A value of α corresponding to 3D-*XY* is held fixed because no convergence is obtained. [c] Parameter values are published in ref 25.

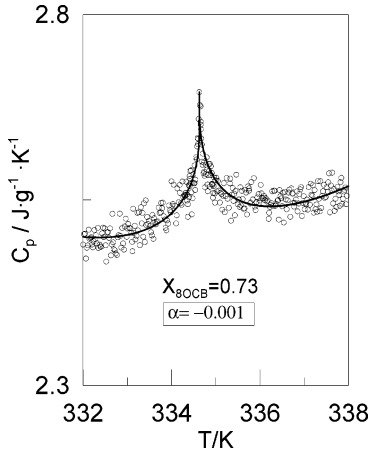

Figure 11. Fit to eq 8 for specific heat data for the mixture X_{8OCB} = 0.73 in the SmA to N second-order transition (heating run). The parameter values are gathered in Table 2.

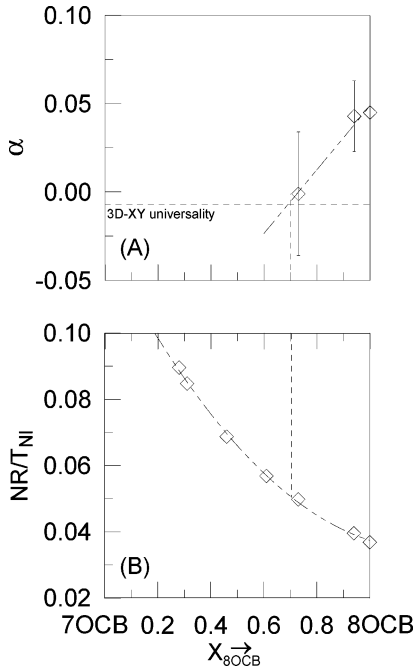

Figure 12. (A) Effective critical exponent α versus composition and (B) the nematic range normalized by the temperature T_{NI} (NR/T_{NI}) against composition for 7OCB + 8OCB mixtures.

lished α-values corresponding to other systems sharing *n*CB and *n*OCB compounds are also included. The data represented in this figure range from the tricritical point (TCP mixtures in the systems 8OCB + 9OCB and 8CB + 9OCB) to nearly 3D-*XY* mixtures (X_{8OCB} = 0.73 in the system 7OCB + 8OCB). A common behavior displayed by this large body of data can be well-represented by the curve

$$\alpha = 397(\mathrm{NR}/T_{NI})^2 - 40.5(\mathrm{NR}/T_{NI}) + 1.02 \qquad (9)$$

The α-value corresponding to the mixture X_{8CB} = 0.56 of the binary system 7CB + 8CB read from reference of Thoen et al.[24] (α = −0.03) was also included in Figure 13 (cross data point).

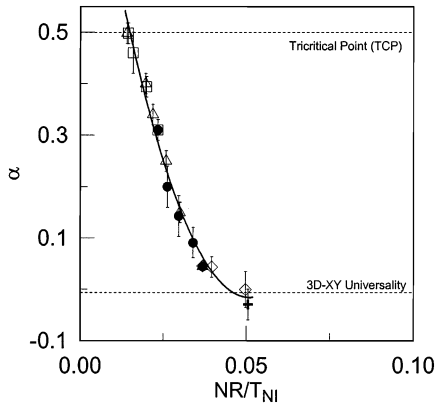

Figure 13. Effective critical exponent α against (NR/T_{NI}) for (◇) 7OCB + 8OCB. The mixtures of (△) 8OCB + 9OCB and (□) 8CB + 9OCB from ref 26 and the mixtures of (●) 8OCB + 8CB from ref 25 are also included. The cross data point is read from ref 24 of Thoen and co-workers. The line corresponds to eq 9.

The goodness of the fit described by eq 9 (see Figure 13) indicates the existence of a common crossover trend for the set of *n*CB and *n*OCB homologous compounds. Notwithstanding the known nonuniversality of the crossover behavior for liquid crystals, eq 9 can nonetheless be used to predict the α-critical exponent from the values of NR/T_{NI} in this particular ensemble of liquid crystals and their mixtures. Therefore, it can be used to predict the order of the SmA to N transition. To do so, only the NR/T_{NI} values (easily obtained from standard calorimetric or optical measurements) are required. In addition, it should be noted that NR/T_{NI} is one minus the McMillan ratio (T_{AN}/T_{NI}), a theoretical parameter that was defined long time ago[28] to quantify the coupling between the nematic and the smectic order parameters.

So, for the homologous series of *n*CB and *n*OCB compounds, and according with eq 9, the SmA to N transition is expected to be 3D-*XY* at NR/T_{NI} of 0.047 (0.953 in McMillan ratio), that is to say, for mixtures richer in 7OCB than $X_{8OCB} \approx 0.7$ (for the system 7OCB + 8OCB) or for mixtures richer in 7CB than $X_{8CB} \approx 0.6$ (for the system 7CB + 8CB). In addition, the SmA to N transition is expected to be tricritical at NR/T_{NI} of 0.015 (0.985 in McMillan ratio). For NR/T_{NI} lower than 0.015, the coupling between the smectic and nematic order parameters is strong enough to obtain a weak first-order SmA to N transition.

7. Concluding Remarks

The two-component system 7OCB + 8OCB provides an excellent example of monotropic reentrant nematic behavior. The experimental phase diagram was established with the aid of MDSC, optical microscopy, and X-ray diffraction measurements. In addition, a complete thermodynamic analysis was performed to reproduce the monotropic reentrant behavior as well as to discuss the stable melting phase diagram. Such

analysis indicates that the isotropic, nematic, and SmA mixtures display almost an ideal behavior with very low excess Gibbs energies. It should be noted that the reentrance behavior is observed because a very small difference in ΔC_p for the pure components exists, even if the phases are ideal.

On the other hand, the order of the SmA to N transition in the aforementioned mixtures was analyzed on the basis of high-resolution specific heat measurements through the well-known renormalization group expression. A relevant result which is obvious in Figure 13 and quantitatively in eq 9 is the uniform and overall crossover trend between 3D-*XY* and TCP behaviors for the *n*CB and *n*OCB series of liquid crystals. Moreover, eq 9 allows us to predict in a simple way the order of the SmA to N transition from standard DSC or optical measurements of the mesophase transitions.

Acknowledgment. The authors are grateful for financial support from the DGE (Grant PB98-0923) and the CIRIT (Fellowship 2001BEAI400080, which allowed D.O.L. to spend some time in the Laboratoire de Chimie Physique, Université Tours, where part of this work was carried out). The authors greatly appreciate the extensive comments by one of the reviewers, which allowed for better understanding of the subject presented in the paper. Finally, the authors are indebted to Prof. R. Rey for helpful discussions about the manuscript and also to Mrs. M. Rodríguez for her help with the English grammar.

References and Notes

(1) Cladis, P. E. *Phys. Rev. Lett*. **1975**, *35* (1), 48.
(2) Cladis, P. E.; Bogardus, R. K.; Daniels, W. B.; Taylor, G. N. *Phys. Rev. Lett.* **1977**, *39* (11), 720.
(3) Cladis, P. E.; Bogardus, R. K.; Aasden, D. *Phys. Rev. A* **1978**, *18* (5), 2292.
(4) Guillon, D.; Cladis, P. E.; Stamatoff, J. *Phys. Rev. Lett*. **1978**, *41* (23), 1598.
(5) Lushington, K. J.; Kasting, G. B.; Garland, C. W. *Phys. Rev. B* **1980**, *22* (5), 2569.
(6) Shashidhar, R.; Ratna, B. R.; Krishna Prasad, S. *Mol. Cryst. Liq. Cryst.* **1985**, *130*, 179.
(7) Ema, K.; Nounesis, G.; Garland, C. W.; Shashidhar, R. *Phys. Rev. A* **1989**, *39*, 2599.
(8) Cladis, P. E. *Mol. Cryst. Liq. Cryst.* **1988**, *165*, 85.
(9) Narayanan, T.; Kumar, A. *Phys. Rep*. **1994**, *249*, 135.
(10) Klug, D. D.; Whalley, E. *J. Chem. Phys.* **1979**, *71*, 1874.
(11) Clark, N. A. *J. Phys., Colloq.* **1979**, *40*, C3−345.
(12) Berker, A. N.; Walker, J. S. *Phys. Rev. Lett*. **1981**, *47* (20), 1469.
(13) Indekeu, J. O.; Berker, A. N.; Chiang, C.; Garland, C. W. *Phys. Rev. A* **1987**, *35* (3), 1371.
(14) Van Hecke, G. R. *J. Phys. Chem.* **1985**, *89*, 2058.
(15) Sorenson, J. M.; Van Hecke, G. R. *J. Phys. Chem.* **1994**, *98*, 10289.
(16) Oonk, H. A. J. *Phase Theory*. *The Thermodynamics of Heterogeneous Equilibria*; Elsevier: Amsterdam, 1981.
(17) Kortan, A. R.; von Känel, H.; Birgenau, R. J.; Litster, J. D. *J. Phys.* **1984**, *45*, 529.
(18) Cladis, P. E.; Guillon, D.; Bouchet, F. R.; Finn, P. L. *Phys. Rev. A* **1981**, *23* (5), 2594.
(19) Brodzik, M.; Dabrowski, R. *Liq. Cryst*. **1995**, *18* (1), 61.
(20) Brodzik, M.; Dabrowski, R. *Liq. Cryst*. **1996**, *20* (1), 99.
(21) Chen, N. R.; Hark, S. K.; Ho, J. T. *Phys. Rev. A* **1981**, *24* (5), 2843.
(22) Urban, S.; Dabrowski, R.; Gestblom, B.; Kocot, A. *Liq. Cryst*. **2000**, *27* (12), 1675.
(23) _ywociński, A. *J. Phys. Chem. B* **1999**, *103*, 3087.
(24) Thoen, J.; Marynissen, H.; van Dael, W. *Phys. Rev. Lett*. **1984**, *52* (3), 204.
(25) Sied, M. B.; López, D. O.; Tamarit, J. Ll.; Barrio, M. *Liq. Cryst.* **2002**, *29* (1), 57.
(26) Sied, M. B.; Salud, J.; López, D. O.; Barrio, M.; Tamarit, J. Ll. *Phys. Chem. Chem. Phys. (PCCP)* **2002**, *4*, 2587.
(27) Kobayashi, K. *Phys. Lett*. **1970**, *31A*, 125.
(28) McMillan, W. L. *Phys. Rev. A* **1971**, *4*, 1238.
(29) De Gennes, P. G.; Prost, J. *The Physics of Liquid Crystals*; Oxford Science Publications: New York, 1994.
(30) Garland, C. W. *Thermochim. Acta* **1985**, *88*, 127.
(31) Iannacchione, G. S.; Finotello, D. *Phys. Rev. E* **1994**, *50* (6), 4780.
(32) Castro, M.; Puértolas, J. A. *Thermochim. Acta* **1997**, *304/305*, 291.
(33) Quian, S.; Iannacchione, G. S.; Finotello, D. *Phys. Rev. E* **1998**, *57* (4), 4305.
(34) Wunderlich, B.; Boller, A.; Okazaki, I.; Kreitmeier, S. *Thermochim. Acta* **1996**, *282/283*, 143.
(35) Hatta, I.; Ichikawa, H.; Todoki, M. *Thermochim. Acta* **1995**, *267*, 83.
(36) Wunderlich, B.; Boller, A.; Okazaki, I.; Ishikiriyama, K. *Thermochim. Acta* **1997**, *304/305*, 125.
(37) Hori, K.; Wu, H. *Liq. Cryst.* **1999**, *26* (1), 37
(38) Zywocinski, A.; Wieczorek, S. A.; Stecki, J. *Phys. Rev. A* **1987**, *36* (4), 1901.
(39) Hulme, D. S.; Raynes, E. P.; Harrison, K. J. *J. Chem. Soc., Chem. Commun*. **1974**, 98.
(40) Oweimreen, G. A.; Morsy, M. A. *Thermochim. Acta* **2000**, *346*, 37.
(41) Blachnik, N.; Kneppe, H.; Shneider, F. *Liq. Cryst.* **2000**, *27* (9), 1219.
(42) Rzoska, S. J.; Ziolo, J.; Sulkowski, W.; Jadzyn, J.; Czechowski, G. *Phys. Rev. E* **2001**, *64*, 052701.
(43) Urban, S.; Gestblom, B.; Würflinger, A. *Mol. Cryst. Liq. Cryst.* **1999**, *331*, 113.
(44) Hori, K.; Koma, Y.; Kurosaki, M.; Itoh, K.; Uekusa, H.; Takenaka, Y.; Ohasahi, Y. *Bull. Chem. Soc. Jpn.* **1996**, *69*, 891.
(45) Kumar, S. *LIQUID CRYSTALS: Experimental Study of Physical Properties and Phase Transitions*; Cambridge University Press: New York, 2001.
(46) Daranas, D.; López, R.; López, D. O. *WINIFIT 2.0 Computer Program*; Polythecnical University of Catalonia: Barcelona, 2000.
(47) Jacobs, M. H. G.; Oonk, H. A. J. *LIQFIT: A computer program for the thermodynamic assessment of T−X liquidus or solidus data*; Utrecht University: Utrecht, The Netherlands, 1990.
(48) van Duijneveldt, J. S.; Baas, F. A. S.; Oonk, H. A. J. *PROPHASE: An MS-DOS program for the calculation of binary T−X phase diagrams*; Utrecht University: Utrecht, The Netherlands, 1988.
(49) López, D. O.; Salud, J.; Tamarit, J. Ll.; Barrio, M.; Oonk, H. A. J. *Chem. Mater*. **2000**, *12*, 1108.
(50) Salud, J.; López, D. O.; Tamarit, J. Ll.; Barrio, M.; Jacobs, M. H. G.; Oonk, H. A. J. *J. Solid State Chem.* **2000**, *154*, 390.
(51) Pardo, L. C.; Barrio, M.; Tamarit, J. Ll.; Negrier, P.; López, D. O.; Salud, J.; Mondieig, D. *J. Phys. Chem. B* **2001**, *105* (42), 10326.
(52) Salud, J.; López, D. O.; Barrio, M.; Tamarit, J. Ll. *J. Mater. Chem.* **1999**, *9*, 909.
(53) Salud, J.; López, D. O.; Barrio, M.; Tamarit, J. Ll.; Oonk, H. A. J. *J. Mater. Chem.* **1999**, *9*, 917.
(54) Salud, J. Ph.D. Thesis, Polytechnic University of Catalonia, 1999.
(55) Garland, C. W.; Meichle, M.; Ocko, B. M.; Kortan, A. R.; Safinya, C. R.; Yu, L. J.; Litster, J. D.; Birgenau, R. J. *Phys. Rev. A* **1983**, *27* (6), 3234.
(56) Quian, S.; Iannacchione, G. S.; Finotello, D. *Mol. Cryst. Liq. Cryst.* **1997**, *292*, 175.
(57) Stine, K. J.; Garland, C. W. *Phys. Rev. A* **1989**, *39* (3), 1482.